JCTC Journal of Chemical Theory and Computation

Article

pubs.acs.org/JCTC

Force Biased Molecular Dynamics Simulation Study of Effect of Dendrimer Generation on Interaction with DNA

Bidisha Nandy,[†] Prabal K. Maiti,[†] and Alex Bunker*[,‡,§]

[†]Center for Condensed Matter Theory, Department of Physics, Indian Institute of Science, Bangalore, India

[‡]Centre for Drug Research, Faculty of Pharmacy, University of Helsinki, Helsinki, Finland

[§]Department of Chemistry, Aalto University, Espoo, Finland

Supporting Information

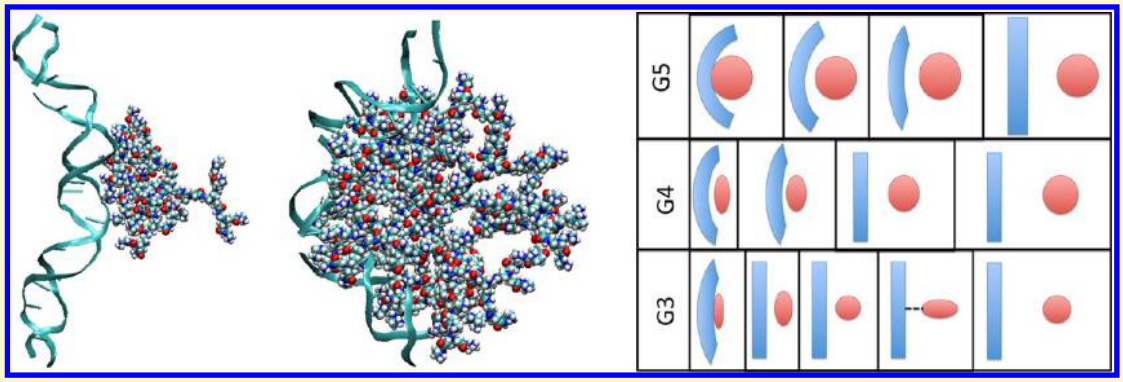

ABSTRACT: We have studied the effect of dendrimer generation on the interaction between dsDNA and the PAMAM dendrimer using force biased simulation of dsDNA with three generations of dendrimer: G3, G4, and G5. Our results for the potential of mean force (PMF) and the dendrimer asphericity along the binding pathway, combined with visualization of the simulations, demonstrate that dendrimer generation has a pronounced impact on the interaction. The PMF increases linearly with increasing generation of the dendrimer. While, in agreement with previous results, we see an increase in the extent to which the dendrimer bends the dsDNA with increasing dendrimer generation, we also see that the deformation of the dendrimer is greater with smaller generation of the dendrimer. The larger dendrimer forces the dsDNA to conform to its structure, while the smaller dendrimer is forced to conform to the structure of the dsDNA. Monitoring the number of bound cations at different values of force bias distance shows the expected effect of ions being expelled when the dendrimer binds dsDNA.

1. INTRODUCTION

Dendrimers are hyper-branched macromolecules with symmetric branching around a central core. The highly controlled architecture of the dendrimer leads to precise control over the molecular weight, number of surface groups, size, and branch mobility. As a result, they have a wide range of biomedical applications,[1] including drug delivery and gene transfection. Gene transfection requires a cationic carrier to bind and compact the negatively charged DNA. Several different synthetic cationic vectors have been used in this role, including lipopolylysine liposomes,[2] block copolymers,[3] transferrin-polycation conjugates,[4] and surface functionalized cationic lipids.[5] Dendrimers formed from branched poly(amido amine),[6] known as PAMAM dendrimers, have shown particular promise as gene transfection agents.[7−12]

The PAMAM dendrimer is, to the lowest order of approximation, a spherical cationic molecule at physiological pH. Thus, when PAMAM dendrimers bind DNA, they can be, at first, thought of as positively charged spheres that wind the negatively charged DNA around them, driven by both (1) the electrostatic interactions and (2) the entropic gain from liberating the bound cations of both the DNA and dendrimer.[13−15] Together,[16,17] the DNA and PAMAM dendrimers form a densely packed nanoscale structure, known as a "dendriplex"[18] with a structural advantage for gene delivery. Experimental evidence has corroborated this picture.[18−21] This is similar to the mechanism through which nucleosomes in the nucleus compact DNA to form the highly ordered chromatin structure,[22] which has been effectively modeled as a negatively charged chain wrapping around positively charged spheres[23,24] with the large scale structure determined by the chain flexibility[25] and the charge density on the chain and spheres.[26] In addition to chromatin, there exist a wide range of similarly structured polyelectrolyte colloid materials.[25−28] Thus, in addition to its role in gene tranfection, the dsDNA−dendrimer complex can be seen as a fundamental system, capable of giving more general insight into polyelectrolyte−colloid complexes.

Received: August 1, 2012
Published: November 14, 2012

   dx.doi.org/10.1021/ct300678r | J. Chem. Theory Comput. 2013, 9, 722−729

Table 1. Simulation Details for the Three Systems Simulated

complex	dendrimer charges	DNA charges	complex charge	number of Cl^- and Na^+ atoms	total atom number in system	number of water molecules	simulation time (ns)
G3 + dsDNA	+32	−74	0.43	32 + 74	179234	58533	24
G4 + dsDNA	+64	−74	0.86	64 + 7	231117	75422	20
G5 + dsDNA	+128	−74	1.72	128 + 74	279023	90580	25

While the model of the positively charged sphere and negatively charged chain has been successful on a large scale, an improved understanding of the microscopic interactions between the individual dsDNA molecule and dendrimer is needed. This would allow us to find ways to alter the design of PAMAM dendrimers to affect the dendriplex structure, and, as a result, enhance gene transfection properties. This has been studied experimentally,[29] and in our past work we have performed all atom simulations of PAMAM dendrimer structure[30−32] and PAMAM dendrimer−DNA complexes,[32,33] in particular the role of the dendrimer generation.[34] We found that the higher the generation of the dendrimer, the greater the extent of DNA bending it produces.

In this study, we continue our investigation of the dendrimer−dsDNA interaction by performing force biased molecular dynamics (MD) simulation. We have used umbrella sampling (US) to determine the PMF for the interactions between dsDNA and G3, G4, and G5 PAMAM dendrimers. Additionally, the dendrimer asphericity and number of bound ions within concentric shells have been calculated as a function of distance along the binding pathway, and snapshots along the pathway have been visualized. A recent study by Mills et al.[35] has calculated the PMF of a G3 dendrimer with DNA; however, they did not study this calculation with dendrimers of varying generation. Our results show that the binding energy increases linearly with increasing generation, and that while the extent to which the dendrimer bends the DNA increases with increasing dendrimer generation, the extent to which the dendrimer structure is deformed by the DNA decreases.

2. METHODS

2.1. Software, Model, and Simulation Parameters. The program "PMEMD" that forms part of the AMBER 9 software package[36] has been used for all MD simulation runs. In all simulations reported in this article, we have used the AMBER 03 force field[37] for the nucleic acid and the Dreiding force field[38] for the dendrimer. We have used the same DNA sequence (GCCGCGAGGTGTCAGGGATTGCAGCC-AGCATCTCGTCG) as used in our previous studies.[32,34,39] The three generations of dendrimers (G3, G4, and G5) were placed into the major groove of the dsDNA molecule using the LEAP module of AMBER 09. In all cases, the initial (3D) structures for the dendrimers were taken from our previous simulations.[31,32] At neutral pH, the G3, G4, and G5 dendrimers have 32, 64, and 128 protonated amines, respectively. The resulting complex was solvated in a 20 Å hydration shell of TIP3P water.[40] The Na^+ counterions were then added to neutralize the negative charges on the phosphate backbone of the DNA. The appropriate number of Cl^- counterions was also added to achieve charge neutrality. For example, for the case of the G3 dendrimer system, 74 Na^+ and 32 Cl^- ions were included in the system, with a total system size of close to 180 000 atoms. The details of the simulation conditions for the three different generations of dendrimer are given in Table 1.

The system was minimized through 1000 steps of steepest descent followed by 2000 steps of conjugate gradient minimization to eliminate any bad contacts. The dsDNA−dendrimer complex was kept fixed using a harmonic constraint with a force constant of 500 kcal/mol/Å throughout the minimization. The system was then heated from 0 to 300 K over 40 ps of MD simulation with a 2 fs time step. During this time the constraint on the dsDNA−dendrimer complex was maintained, but with a reduced force constant of 20 kcal/mol/Å. All covalent bonds involving the hydrogen atoms were subjected to SHAKE constraints[41] using a geometrical tolerance of 5×10^{-4} Å. The MD simulation was then carried out at constant temperature and pressure (NpT) using Berendsen weak coupling[42] (0.5 ps time constant for heat bath coupling and 0.2 ps pressure relaxation time) for both the thermostat and barostat for 50 ps, with the harmonic constraint reducing from 20 kcal/mol/Å to zero in steps of 5 kcal/mol/Å. The system was then equilibrated at 300 K using unconstrained NpT MD for 100 ps. For the electrostatic interactions, we employed the particle mesh Ewald method,[43,44] with a cubic B-spline interpolation of order 4, a 10^{-4} tolerance set for the direct space sum cutoff and a real space cutoff of 9 Å. Van der Waals interactions were also computed using a real space cutoff of 9 Å, and with a nonbond list update frequency of 10. The same protocol has been followed in our previous simulations.[32,33] Finally 20−30-ns-long constant number volume and temperature (NVT) MD was performed on all systems before starting the force biased MD simulations, discussed in the following section.

2.2. US to Determine PMF of Binding between Dendrimer and DNA. Force biased MD involves performing MD simulation with an externally applied force $\vec{F}_{fb}$ exerted on either a single atom or the center of mass of a group of atoms. US[45,46] involves performing a set of simulations at a set of harmonic force biases, each constraining the distance between two sets of atoms within the system. Each of these separate force bias values is referred to as a "window". Each window has a value of harmonic force constant k_i and distance r_i. The values of k_i for each of the windows are independent and can be separately set to optimize the sampling of phase space. If the simulation is performed at a set of windows that are close enough for there to be sufficient overlap between the phase space sampled in adjacent windows, then the PMF along the reaction path can be calculated using the weighted histogram analysis method (WHAM).[47] We have successfully used this method to calculate the PMF along different possible pathways to the active site of the protein prolyl oligopeptidase (POP) in a previous publication.[48]

The US method was used to calculate the PMF of the interaction between dendrimers of generations G3, G4, and G5 and DNA. Using the center of mass of all atoms for either the DNA or dendrimer molecule as the two atom groups was not possible due to memory constraints. We thus selected an appropriate subset of atoms to achieve the same effect. For the case of the DNA, this was chosen to be the phosphate atoms

dx.doi.org/10.1021/ct300678r | J. Chem. Theory Comput. 2013, 9, 722−729

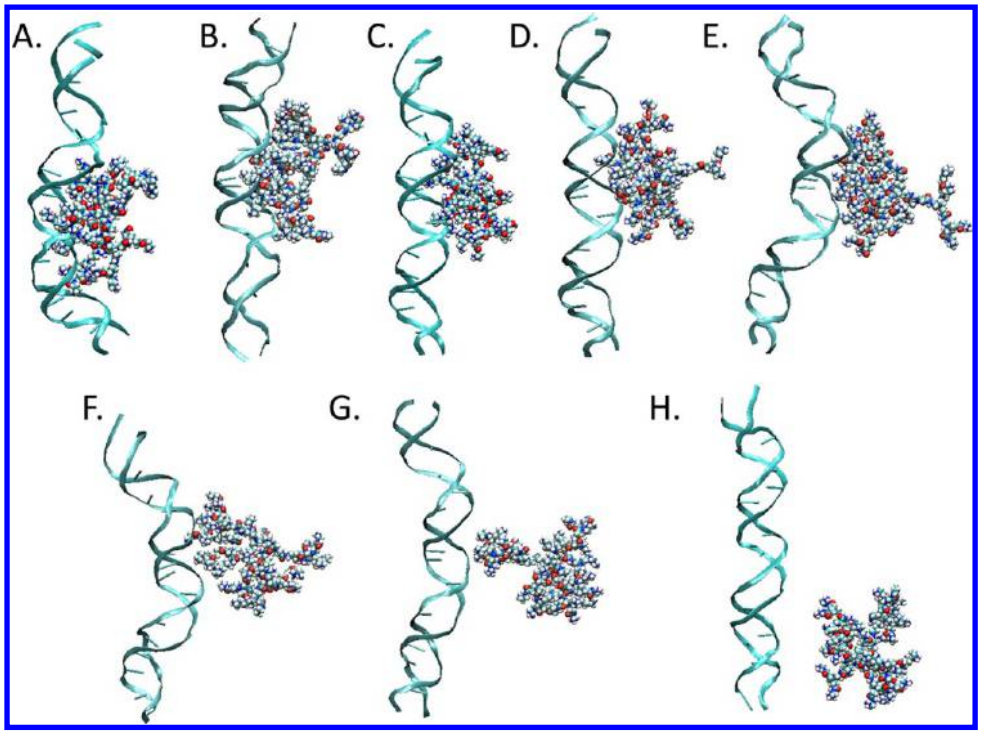

Figure 1. The final frame of the PMF windows for the G3 dendrimer at (A) no force bias, (B) 2.0 nm, (C) 2.5 nm, (D) 3.0 nm, (E) 3.5 nm, (F) 4.0 nm, (G) 4.5 nm, and (H) 5.0 nm.

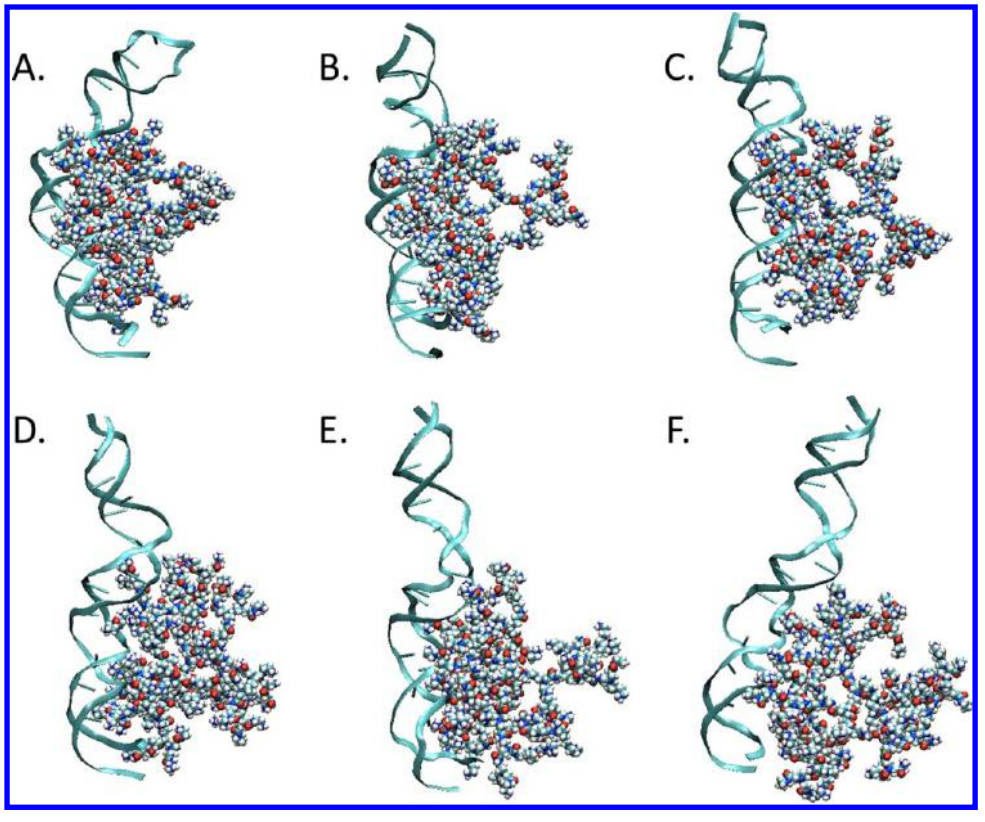

Figure 2. The final frame of the PMF windows for the G4 dendrimer at (A) no force bias, (B) 2.0 nm, (C) 2.5 nm, (D) 3.0 nm, (E) 3.5 nm, and (F) 4.0 nm.

since these represent the most rigid structural element of the DNA. For the G3 dendrimer, we selected all atoms on the inner two generations, and for the G4 and G5 dendrimer, we selected all the nitrogen atoms in the inner first through third and first through fourth subgenerations, respectively. In order to avoid the dendrimer adapting to the constraint by simply rolling along the DNA, extra constraints needed to be applied. The phosphate atoms of the DNA were divided into five sections,

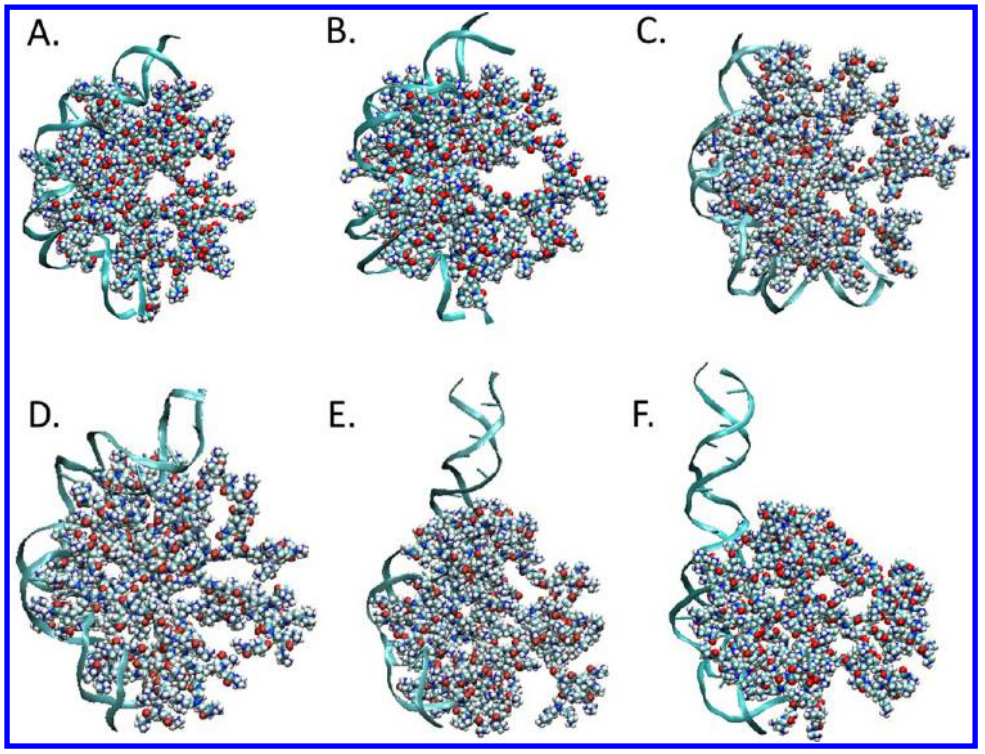

Figure 3. The final frame of the PMF windows for the G5 dendrimer at (A) no force bias, (B) 2.0 nm, (C) 2.5 nm, (D) 3.0 nm, (E) 3.5 nm, and (F) 4.0 nm.

and a purely repulsive interaction between the center of mass of each of these sets of atoms and the aforementioned dendrimer atoms was applied for any distance below $r_i - 0.5$ nm. The simulation was performed at a set of windows ranging up to 4 nm for the G4 and G5 dendrimers and 5 nm for the G3 dendrimer, and the PMF was calculated out to this distance. In each case, we first observed the time taken for the system to attain the new equilibrium distance. The system was deemed to have reached equilibrium, concerning the properties we investigate, and analysis was performed on the remaining trajectory. The separation of the windows where the MD was performed was selected as either 1 or 2 nm, dependent on the sampling requirements in the region of the given windows. The number of windows used, their k_i and r_i values, and the verification that this set of windows samples the phase space fully are included in the Supporting Information.

2.3. Calculation of Asphericity Parameter. In previous work,[32,49] we have determined that the dendrimer molecule, normally approximately spherical, undergoes a shape distortion, bending, when binding to dsDNA. The extent of this bending can be quantified in terms of the asphericity of the dendrimer molecule. According to Rudnick and Gaspari,[50] the asphericity parameter is defined as

$$\delta = 1 - 3(\langle I_1 \rangle / \langle I_2^2 \rangle) \quad (1)$$

where

$$I_1 = I_x I_y + I_y I_z + I_x I_z \quad (2)$$

$$I_2 = I_x + I_y + I_z \quad (3)$$

and I_x, I_y, and I_z are the three eigenvalues of the shape tensor **G** in ascending order. The average asphericity was calculated in each simulation window for all of the systems simulated.

3. RESULTS

Snapshots along the binding pathway (varying the force bias distance) are shown in Figure 1 for the G3 dendrimer−DNA system, in Figure 2 for the G4−dendrimer system, and in Figure 3 for the G5 dendrimer−DNA system. It can be seen that with increasing dendrimer generation, the degree to which the structure of the DNA is altered, notably the bending of the DNA helical axis, increases. For the G3 dendrimer, it can be seen that we have been able to completely separate the dendrimer from the DNA at a force bias distance of 5 nm, the distance between dendrimer and DNA clearly beyond the screening distance. Our results for the G4 and G5 dendrimers show that we still have contact between DNA and the dendrimer at the farthest window (4 nm); however, we see the overall structure of the dendrimer has lost its deformation due to the DNA at this distance. It was not computationally feasible to simulate the system with a simulation size large enough to extend the G4 and G5 simulations any further. We can thus expect to have sampled the full PMF for the case of the G3 dendrimer, but not for the case of the G4 and G5 dendrimers.

The potential of mean force graph is shown in Figure 4. We see, as expected from our visualization of the simulation, that we have sampled the full pathway for the case of the G3 dendrimer, but not for the case of the G4 and G5 dendrimers. For the G3 dendrimer, the binding potential increases approximately linearly; then, at a separation of ∼4 nm the energy levels out, indicating that the dendrimer has been effectively separated from the DNA. For the G4 and G5 dendrimers, this pathway has clearly not been sampled to the end; however, from what we have observed, we are able to determine a clear conclusion: the binding energy, i.e., the height of the PMF barrier, varies linearly with the dendrimer generation. In addition, we see a qualitative difference between the PMF graph for the G3 dendrimer vs the G4 and G5

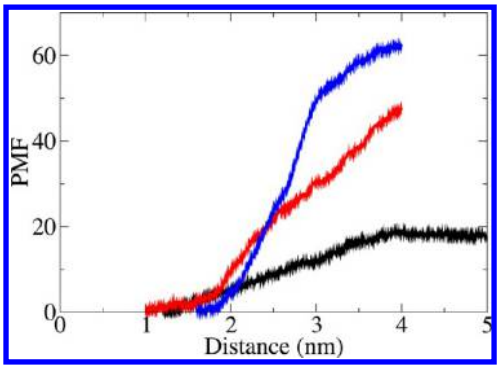

Figure 4. Potential of mean force for G3 (black line), G4 (red line), and G5 (blue line) dendrimers. Note that G5 has clearly reached the equilibrium distance. Increasing the generation of the dendrimer clearly substantially increases the binding energy, approximately linearly with the generation.

dendrimers. For the G3 dendrimer, we see a linear rise from the equilibrium distance continuing until the end of the potential pathway at 4 nm. For the G4 and G5 dendrimers, we see an initial region of a rise with what looks like an exponent greater than unity, followed by a crossover into a more gently sloping linear rising region. For the G4 dendrimer system, this crossover occurs at a separation of ∼2.3 nm, and for the G5 system, at ∼2.9 nm.

The number of ions within four concentric shells of the dendrimer for both Cl^- anions and Na^+ cations as a function of force bias distance is shown in Figure 5. The number of Cl^- anions within the four distance shells (3, 5, 7, and 8.5 nm) at all distances approximately doubles with each increase in generation of the dendrimer; however, for the Na^+ cations, this number decreases slightly with increasing generation of the dendrimer. Most interesting in this measurement is the change in this number with force bias distance. For the Cl^- anions, the number rises slightly for all distance shells; however, for the case of the Na^+ cations, we see that this rise only occurs within 5 nm for the G3 dendrimer, within 7 nm for the G4 dendrimer, and for all shells for the G5 dendrimer.

The results for the asphericity of the dendrimers along the force bias pathway, shown in Figure 6, provide yet another

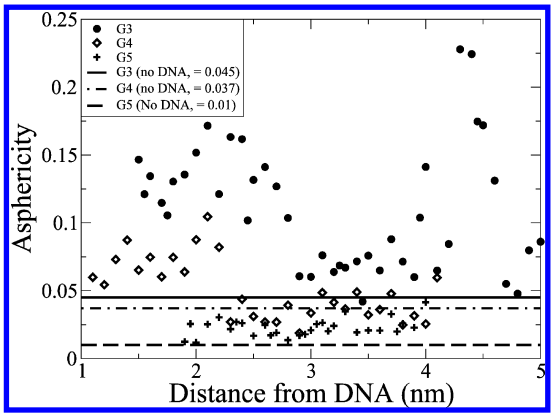

Figure 6. Aspericity of G3, G4, and G5 dendrimers. The deformation of the dendrimer is inversely related to the generation.

window into the structural changes involved in the DNA dendrimer binding. In previous publications[49,51] we determined that, in the absence of DNA, the asphericity of the G3, G4, and G5 dendrimers are 0.045, 0.037, and 0.01, respectively. Our results show that, for the case of the G5 dendrimer, the asphericity does not change as the dendrimer distance from the DNA is increased, remaining constant at a value of ∼0.02, slightly larger than the measured value in absence of DNA. For the G3 and G4 dendrimers, we see evidence of an increased asphericity when the dendrimer is close to the DNA, a constant value of ∼0.14 out to ∼2.2 nm for the G3 dendrimer and ∼0.075 out to ∼2.8 nm for the G4 dendrimer. For the G4 dendrimer, the asphericity drops to approximately the value in the absence of DNA (0.037) and remains constant, while for the G3 dendrimer the asphericity drops to a value of ∼0.07,

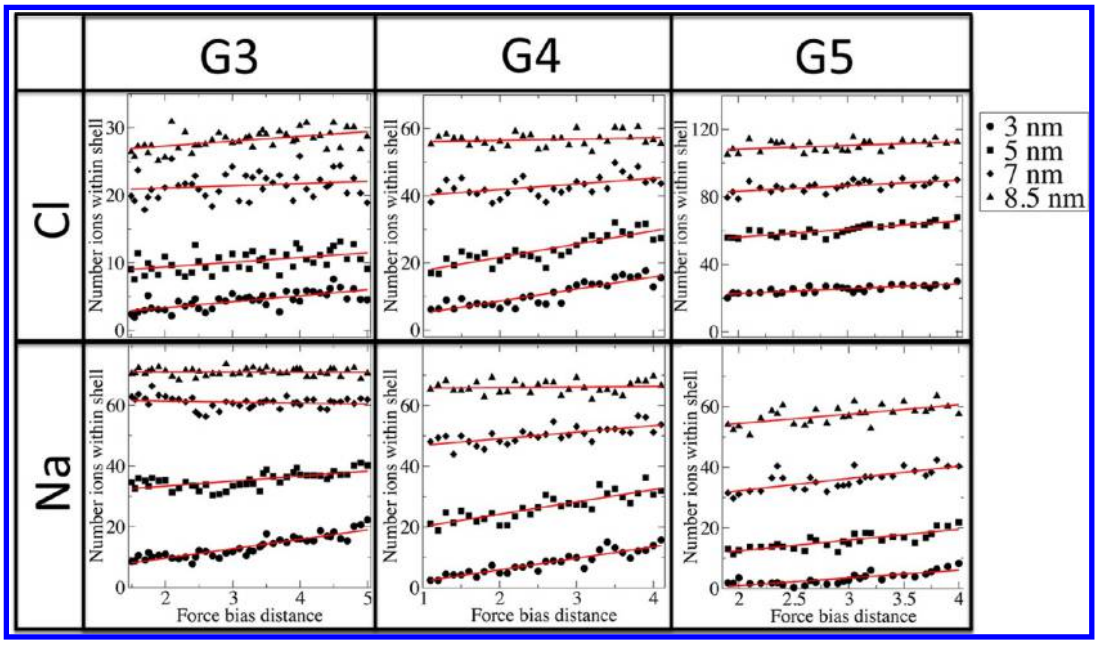

Figure 5. Bound ions in four concentric shells for all dendrimer systems for both Cl^- and Na^+ ions. Note that the scale is constant for all three dendrimers for the case of the Na^+ cations but is doubling with each generation for the Cl^- anions.

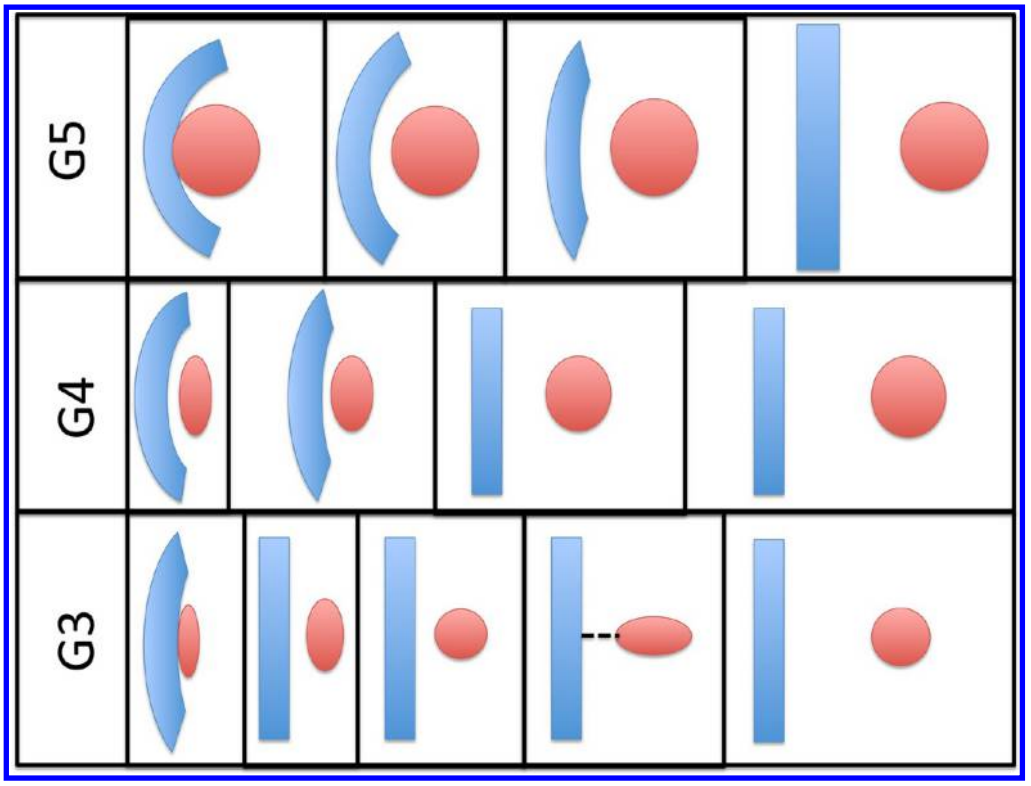

Figure 7. Schematic showing the effect of dendrimer generation on the interaction between DNA and dendrimer. For the G5 dendrimer, there is no noticeable deformation of the dendrimer in the asphericity results; however the DNA was observed to bend, observed both visually and in the steep quadratic region of the PMF. For the G4 dendrimer, both the DNA and the dendrimer were observed to deform. For the G3 dendrimer the DNA deformed very little, but the dendrimer underwent considerable deformation on contact with the DNA. Also a peak in the asphericity result further away from the dendrimer was the result of the final few water bridges holding while the rest of the dendrimer pulls away.

slightly larger than the asphericity in the absence of DNA (0.045), then shows a sharp peak at a distance of ~4.4 nm before dropping down to the approximate range of the value in the absence of DNA.

4. DISCUSSION

Our results show a molecular level picture for the binding mechanism and interaction between dendrimer and DNA. For larger generation dendrimers, the extent of DNA bending is known to increase, as has been shown in our previous simulations,[34] and experimentally by Chen et al.[18] We find that the number of bound anions within the cell increases, within the four distance shells we defined, when the force biased distance increases. This supports the mechanism demonstrated in both our[31] and others'[19] previous research: DNA−dendrimer binding is, at least in part, driven by the entropic gain resulting from the release of counterions. Our result that the number of bound anions doubles with each increase in dendrimer generation is due to the addition of each new dendrimer generation doubling the positive charge of the dendrimer. The small decrease in the number of cations within each binding radius with increasing generation of dendrimer indicates stronger binding of dsDNA with the more protonated dendrimer.

Concerning the PMF calculation, we see the clear result that binding energy increases approximately linearly with increasing generation of the dendrimer. In addition, while for the G3 dendrimer there is just a single region of linearly increasing potential energy, for the G4 and G5 dendrimers, we see a crossover from an increase with what looks like an exponent greater than unity to a slower linear increase. A possible explanation of these results can be found in our visualization of the DNA−dendrimer complexes at different force bias distances. We see that for the G3 dendrimer the DNA is only slightly bent, the dendrimer conforming to the DNA, while for the G5 dendrimer, it is the dendrimer that forces the DNA to conform to it, bending the DNA around it. This provides an explanation for the different nature of the PMF curves for the G3 and higher generation dendrimers: For the G3 dendrimer, we see a predominantly electrostatic effect with the energy changing linearly as the DNA and dendrimer are separated. For the higher generation dendrimers, however, as the dendrimer is separated from the DNA, initially at short distances the DNA is straightening, leading to an additional factor in the binding energy. The crossover into linear behavior indicates that the DNA has straightened out, and we only see the same electrostatic effects as in the G3 dendrimer at these larger distances. It can be hypothesized that the increase in the binding energy of the dendrimer with increasing dendrimer generation results from the increased bending of the DNA that is evident.

While our PMF results can be explained by an increasing extent of bending in the DNA structure with increasing dendrimer generation, our dendrimer asphericity results indicate an inverse relationship with generation regarding the deformation of the dendrimer. For the G5 dendrimer, we see no evidence of the dendrimer being deformed by the DNA; the G5 dendrimer has an asphericity that is constant with respect to force bias distance. The larger asphericity value, than that measured for the G5 dendrimer without the DNA present, can

be attributed to the limited accuracy of asphericity measurements. For the G4 dendrimer, we see a drop in asphericity from a higher value to approximately the value measured without the DNA present, indicating an increased deformation of the dendrimer onto the DNA when closer than 2.2 nm. For the G3 dendrimer, we see the same drop in asphericity; however at a force bias distance of ∼4.4 nm, we see a sharp peak. An explanation of this can be found from observation of the DNA−dendrimer complex at approximately this distance, shown in Figure 1G: the dendrimer is small enough that a single terminus has not broken its water bridge to the DNA, thus stretching out the dendrimer as it is pulled away. When pulled farther, this final water bridge breaks, and the asphericity drops to approximately the value found in the absence of DNA.

Combining the asphericity measurements and the PMF calculations, and using our visualization of the DNA dendrimer complex at different force bias distances to supplement these results, we have a picture of the DNA−dendrimer interaction that can be summarized as follows: for the smaller, lower generation dendrimers, it is the DNA that conforms the dendrimer to fit it, and for the larger, higher generation dendrimers, it is the dendrimer that conforms the DNA to fit its structure, bending the DNA. A schematic of the picture of this interaction our results combine to present is shown in Figure 7.

The section of dsDNA simulated is limited by the finite size of the simulation box that is tractable with currently available computational resources. The purpose of our simulation is to investigate the interaction between a short segment of dsDNA and dendrimer. With this finite length of the DNA, we cannot test the bead-on-string model of the DNA−dendrimer complex, proposed on the basis of experimental results. This would require a simulation involving a much longer length of DNA, which we plan to carry out in the future.

5. CONCLUSION

We performed a set of forced biased simulations along the binding pathway between a dendrimer and DNA for PAMAM dendrimers of generation G3, G4, and G5. We used US across this pathway to calculate the PMF along the binding pathway. Our results clearly show that PMF increases approximately linearly with increasing generation of the dendrimer, in disagreement with a previous study by Mills et al. We calculated the number of both Na^+ cations and Cl^- anions within four concentric binding shells for all three dendrimer generations studied and determined that, while we see the expected phenomenon of some ions being expelled from the dendrimer when binding the DNA, for the case of the cations, but not the anions, this only occurs out to a certain distance, which increases with increasing generation of the dendrimer. Combining the results for PMF, dendrimer asphericity, and visualization of the DNA−dendrimer complex along the force bias pathway shows that for the smaller, lower generation dendrimers, it is the DNA that alters the conformation of the dendrimer when they complex, but for the larger, higher generation dendrimer it is the dendrimer that alters the conformation of the DNA, causing it to bend around the dendrimer.

■ ASSOCIATED CONTENT

Supporting Information

Information about (a) the simulation windows included and sampling of phase space, (b) verication of results through repeats of simulation from separate starting points, and (c) major groove width calculation. This information is available free of charge via the Internet at http://pubs.acs.org/.

■ AUTHOR INFORMATION

Corresponding Author

*E-mail: alex.bunker@helsinki.fi.

Notes

The authors declare no competing financial interest.

■ ACKNOWLEDGMENTS

This work was supported by the Academy of Finland (A.B.) and DST India. Computational resources have been provided by the DST Centre for Mathematical Biology at IISc and the Finnish IT Centre for Science Ltd. (CSC).

■ REFERENCES

(1) Svenson, S.; Tomalia, D. A. *Adv. Drug Delivery Rev.* **2005**, *57*, 2106−2129.
(2) Zhou, X.; Huang, L. *Biochim. Biophys. Acta* **1994**, *1189*, 195−203.
(3) Wolfert, M. A.; Schacht, E. H.; Toncheva, V.; Ulbrich, K.; Nazarova, O.; Seymour, L. W. *Hum. Gene Ther.* **1996**, *7*, 2123−2133.
(4) Wagner, E.; Cotten, M.; Foisner, R.; Birnstiel, M. L. *Proc. Natl. Acad. Sci. U. S. A.* **1991**, *88*, 4255−4259.
(5) Martin-Herranz, A.; Ahmad, A.; Evans, H. M.; Ewert, K.; Schulze, U.; Safinya, C. R. *Biophys. J.* **2004**, *86*, 1160−1168.
(6) Wang, R.; Zhou, L.; Zhou, Y.; Li, G.; Zhu, X.; Gu, H.; Jiang, X.; Li, H.; Wu, J.; He, L.; Guo, X.; Zhu, B.; Yan, D. *Biomacromolecules* **2010**, *11*, 489−495.
(7) Bielinska, A.; Kukowska-Latallo, J. F.; Johnson, J.; Tomalia, D. A.; James R. Baker, J. *Nucleic Acids Res.* **1996**, *24*, 2176−2182.
(8) Haensler, J.; Szoka, F. C., Jr. *Bioconjugate Chem.* **1993**, *4*, 372−379.
(9) Kabanov, V. A.; Zezin, A. B.; Rogacheva, V. B.; Gulyaeva, Z. G.; Zansochova, M. F.; Joosten, J. G. H.; Brackman, J. *Macromolecules* **1998**, *31*, 5142−5144.
(10) Kukowska-Latallo, J. F.; Bielinska, A. U.; Johnson, J.; Spindler, R.; Tomalia, D. A.; Baker, J. A., Jr. *Proc. Natl. Acad. Sci. U. S. A.* **1996**, *93*, 4897−4902.
(11) Bielinska, A. U.; Chen, C.; Johnson, J.; Baker, J. R., Jr. *Bioconjugate Chem.* **1999**, *10*, 843−850.
(12) Tang, M. X.; Redemann, C. T.; Szoka, F. C., Jr. *Bioconjugate Chem.* **1996**, *7*, 703−714.
(13) Welch, P.; Muthukumar, M. *Macromolecules* **2000**, *33*, 6159−6167.
(14) Ou, Z.; Muthukumar, M. *J. Chem. Phys.* **2006**, *124*, 154902.
(15) Muthukumar, M. *J. Chem. Phys.* **2004**, *120*, 9343.
(16) Pavan, G. M.; Danani, A.; Pricl, S.; Smith, D. K. Modeling the multivalent recognition between dendritic molecules and DNA - understanding how ligand sacrifice and shielding may enhance binding. *J. Am. Chem. Soc.* **2009**, *131*, 9686−9694.
(17) Pavan, G. M.; Danani, A. The influence of dendron's architecture on the "rigid" and "flexible" behaviour in Binding DNA - a modelling study. *Phys. Chem. Chem. Phys.* **2010**, *12*, 13914−13917.
(18) Chen, C.-Y.; Su, C.-J.; Peng, S.-F.; Chen, H.-L.; Sung, H.-W. *Soft Matter* **2011**, *7*, 61−63.
(19) Evans, H. M.; Ahmad, A.; Ewert, K.; Pfohl, T.; Martin-Herranz, A.; Bruinsma, R. F.; Safinya, C. R. *Phys. Rev. Lett.* **2003**, *91*, 075501.
(20) Su, C.-J.; Liu, Y.-C.; Chen, H.-L.; Li, Y.-C.; Lin, H.-K.; Liu, W.-L.; Hsu, C.-S. *Langmuir* **2007**, *23*, 975−978.
(21) Froehlich, E.; Mandeville, J. S.; Weinert, C. M.; Kreplak, L.; Tajmir-Riahi, H. A. *Biomacromolecules* **2011**, *12*, 511−517.
(22) Schiessel, H. *J. Phys.: Condens. Matter* **2003**, *15*, R699−R774.
(23) Zinchenko, A. A.; Yoshikawa, K.; Baigl, D. *Phys. Rev. Lett.* **2005**, *95*, 228101.
(24) Kunze, K.-K.; Netz, R. R. *Phys. Rev. Lett.* **2000**, *85*, 4389−4392.
(25) Jonsson, M.; Linse, P. *J. Chem. Phys.* **2001**, *115*, 10975−10985.
(26) Jonsson, M.; Linse, P. *J. Chem. Phys.* **2001**, *115*, 3406−3418.

(27) Grosberg, A. Y.; Nguyen, T. T.; Shklovskii, B. I. *Rev. Mod. Phys.* **2002**, *74*, 329−345.
(28) Decher, G. *Science* **1997**, *277*, 1232−1237.
(29) Bielinska, A. U.; Kukowska-Latallo, J. F.; Baker, J. R., Jr. *Biochim. Biophys. Acta* **1997**, *1353*, 180−190.
(30) Maiti, P. K.; Goddard, W. A., III. *J. Phys. Chem. B* **2006**, *110*, 25628−25632.
(31) Maiti, P. K.; Messina, R. *Macromolecules* **2008**, *41*, 5002−5006.
(32) Maiti, P. K.; Bagchi, B. *Nano Lett.* **2006**, *7*, 2478−2485.
(33) Vasumathi, V.; Maiti, P. K. *Macromolecules* **2010**, *43*, 8264−8274.
(34) Nandy, B.; Maiti, P. K. *J. Phys. Chem. B* **2011**, *115*, 217−230.
(35) Mills, M.; Orr, B.; Banaszak, M. M.; Andricioaei, I. *Biophys. J.* **2010**, *98*, 834−842.
(36) Case, D. A.; Darden, T. A.; Cheatham, T. E., III; Simmerling, C. L.; Wang, J.; Duke, R. E.; Luo, R.; Merz, K. M.; Pearlman, D. A.; Crowley, M.; Walker, R. C.; Zhang, W.; Wang, B.; Hayik, S.; Roitberg, A.; Seabra, G.; Wong, K. F.; Paesani, F.; Wu, X.; Brozell, S.; Tsui, V.; Gohike, H.; Yang, L.; Tan, C.; Mongan, J.; Hornak, V.; Beroza, P.; Mathews, D. H.; Ross, W. S.; Kollman, P. A. *AMBER 9*; University of California: San Francisco, CA, 2006.
(37) Duan, Y.; Wu, C.; Chourdhury, S.; Lee, M. C.; Xiong, G.; Zhang, W.; Yang, R.; Cieplak, P.; Luo, R.; Lee, T.; Caldwell, J.; Wang, J.; Kollman, P. A. *J. Comput. Chem.* **2003**, *24*, 1999−2012.
(38) Mayo, S. L.; Olafson, B. D.; Goddard, W. A., III. *J. Phys. Chem.* **1990**, *94*, 8897−8909.
(39) Santosh, M.; Maiti, P. K. *Biophys. J.* **2011**, *101*, 1393−1402.
(40) Jorgensen, W. L.; Chandrasekhar, J.; Madura, J. D.; Impey, R. W.; Klein, M. L. *J. Chem. Phys.* **1983**, *79*, 926−935.
(41) Ryckaert, J.; Ciccotti, G.; Berendsen, H. J. C. *J. Comput. Phys.* **1977**, *23*, 327−341.
(42) Berendsen, H. J. C.; Postma, J. P. M.; van Gunsteren, W. F.; DiNola, A.; Haak, J. R. *J. Chem. Phys.* **1984**, *81*, 3684−3690.
(43) Essman, U.; Perela, L.; Berkowitz, M. L.; Darden, H. L.; Pedersen, L. G. *J. Chem. Phys.* **1995**, *103*, 8577−8592.
(44) Karttunen, M.; Rottler, J.; Vattulainen, I.; Sagui, C. In *Current Top. Membr.*; Feller, S., Ed.; Elsevier: Amsterdam, 2008; Vol. *60*; pp 49 − 89.
(45) Roux, B. *Comput. Phys. Commun.* **1995**, *91*, 275−282.
(46) Torrie, G. M.; Valleau, J. P. *J. Comput. Phys.* **1977**, *23*, 187−199.
(47) Kumar, S.; Bouzida, D.; Swendsen, R. H.; Kollman, P. A.; Rosenberg, J. M. *J. Comput. Chem.* **1992**, *13*, 1011−1021.
(48) St. Pierre, J.-F.; Karttunen, M.; Mousseau, N.; Róg, T.; Bunker, A. *J. Chem. Theory Comput.* **2011**, *7*, 1583−1594.
(49) Maiti, P. K.; Li, Y.; Cagin, T.; Goddard, W. A., III. *J. Chem. Phys.* **2009**, *120*, 144902.
(50) Rudnick, J.; Gaspari, G. *J. Phys. A: Math Gen.* **1986**, *19*, L191.
(51) Maiti, P. K.; Cagin, T.; Lin, S.-T.; Goddard, W. A., III. *Macromolecules* **2005**, *38*, 979−991.